

**Hyperbaric Oxygen Therapy Influence on Irradiated Bone Repair and Collagen
Orientation**

**Influência da oxigenação hiperbárica no reparo ósseo e organização do colágeno após
radioterapia**

**Influencia de la terapia de oxígeno hiperbárico en la reparación ósea y la orientación del
colágeno después de la radioterapia**

Received: 11/05/2020 | Reviewed: 11/08/2020 | Accept: 11/16/2020 | Published: 11/20/2020

Flaviana Soares Rocha

ORCID: <https://orcid.org/0000-0002-6759-2229>

University of Brasília, Brazil

E-mail: flavianasoares.rocha@gmail.com

Layra Gabriella Pereira de Rezende

ORCID: <https://orcid.org/0000-0002-2692-9163>

Federal University of Uberlândia, Brazil

E-mail: layragabriella3@hotmail.com

Danyella Carolyna Soares dos Reis

ORCID: <https://orcid.org/0000-0002-8548-0538>

Federal University of Uberlândia, Brazil

E-mail: danyellacsoaresr@gmail.com

Gustavo Davi Rabelo

ORCID: <https://orcid.org/0000-0001-9511-5078>

Federal University of Santa Catarina, Brazil

E-mail: drgustavorabelo@yahoo.com.br

Letícia de Souza Castro Filice

ORCID: <https://orcid.org/0000-0003-4300-1575>

Federal University of Uberlândia, Brazil

E-mail: leticiafilice@gmail.com

Darceny Zanetta-Barbosa

ORCID: <https://orcid.org/0000-0002-8755-0931>

Federal University of Uberlândia, Brazil

E-mail: darceny_@hotmail.com

Paula Dechichi

ORCID: <https://orcid.org/0000-0001-5509-8138>

Federal University of Uberlândia, Brazil

E-mail: pauladechichi@ufu.br

Abstract

The present study aimed to evaluate the effects of HBO on bone repair after ionizing radiation, by using histomorphometry, computed tomography and polarization microscopy. Twenty male Wistar rats were used. One radiation dose (30 Gy) was administered on the left leg in all animals, and after 30 days, bone defects were created in both femurs. Then, 10 animals received daily HBO sessions (2.5 ATA for 90 minutes), and all animals were euthanized 5 or 7 days after surgery. The femurs were separated into 4 groups (n=5) for each euthanasia time interval: Control (Right femur: Non-irradiated and Non-HBO), RXT (Left femur: Irradiated and Non-HBO), HBO (Right femur: Non-irradiated with HBO), RXT+HBO (Left femur: Irradiated with HBO). The bone cortical and defects were evaluated. Data were analyzed using the Kolmogorov-Smirnov tests, unpaired t-test, and ANOVA with Bonferroni correction. Higher HU values and new bone formation were observed in Control and HBO groups, with improved repair. Group HBO showed predominant Yellow/Orange/Red birefringence of collagen in the defect area. HBO improved bone repair in physiological conditions, with increased blood vessels and bone formation. However, it was not efficient in improving repair and collagen orientation in bone after high doses of ionizing radiation.

Keywords: Ionizing radiation; Hyperbaric oxygenation; Osteogenesis; Collagen.

Resumo

O presente estudo teve como objetivo avaliar os efeitos da HBO no reparo ósseo após radiação ionizante, por meio da histomorfometria, tomografia computadorizada e microscopia de polarização. Vinte ratos Wistar machos foram usados. Uma dose de radiação (30 Gy) foi administrada na perna esquerda em todos os animais, e após 30 dias, defeitos ósseos foram criados em ambos os fêmures. Em seguida, 10 animais receberam sessões diárias de HBO (2,5 ATA por 90 minutos), e todos os animais foram sacrificados 5 ou 7 dias após a cirurgia. Os fêmures foram separados em 4 grupos (n = 5) para cada intervalo de tempo de eutanásia: Controle (fêmur direito: não irradiado e não HBO), RXT (fêmur esquerdo: irradiado e não HBO), HBO (fêmur direito: não-irradiado com HBO), RXT + HBO (fêmur esquerdo: irradiado com HBO). A cortical óssea e os defeitos foram avaliados. Os dados foram

analisados por meio dos testes de Kolmogorov-Smirnov, teste t não pareado e ANOVA com correção de Bonferroni. Valores maiores de HU e neoformação óssea foram observados nos grupos Controle e HBO, com melhora do reparo. O grupo HBO apresentou birrefringência de colágeno predominantemente amarela/laranja/vermelha na área do defeito. A HBO melhorou a reparação óssea em condições fisiológicas, com aumento dos vasos sanguíneos e formação óssea. No entanto, não foi eficiente em melhorar o reparo e a orientação do colágeno no osso após altas doses de radiação ionizante.

Palavras-chave: Radiação ionizante; Oxigenação hiperbárica; Osteogênese; Colágeno.

Resumen

El presente estudio tuvo como objetivo evaluar los efectos de la HBO en la reparación ósea después de la radiación ionizante, mediante el uso de histomorfometría, tomografía computarizada y microscopía de polarización. Se utilizaron veinte ratas Wistar macho. Se administró una dosis de radiación (30 Gy) en la pierna izquierda en todos los animales y, después de 30 días, se crearon defectos óseos en ambos fémures. Luego, 10 animales recibieron sesiones diarias de HBO (2,5 ATA durante 90 minutos), y todos los animales fueron sacrificados 5 o 7 días después de la cirugía. Los fémures se separaron en 4 grupos (n = 5) para cada intervalo de tiempo de eutanasia: Control (fémur derecho: no irradiado y no HBO), RXT (fémur izquierdo: irradiado y no HBO), HBO (fémur derecho: no HBO) - irradiado con HBO), RXT + HBO (fémur izquierdo: irradiado con HBO). Se evaluaron la cortical ósea y los defectos. Los datos se analizaron mediante las pruebas de Kolmogorov-Smirnov, la prueba t para datos no apareados y ANOVA con corrección de Bonferroni. Se observaron valores más altos de HU y formación de hueso nuevo en los grupos Control y HBO, con una mejor reparación. El grupo HBO mostró una birrefringencia predominante de colágeno amarillo / naranja / rojo en el área del defecto. HBO mejoró la reparación ósea en condiciones fisiológicas, con aumento de los vasos sanguíneos y la formación de hueso. Sin embargo, no fue eficaz para mejorar la reparación y la orientación del colágeno en el hueso después de altas dosis de radiación ionizante.

Palabras clave: Radiación ionizante; Oxigenación hiperbárica; Osteogénesis; Colágeno.

1. Introduction

Radiotherapy in oral cancer treatment can generate unwanted side effects because ionizing radiation cannot distinguish tumor cells from healthy cells (Lerouxel et al., 2009;

Chouinard et al., 2016; Sroussi et al., 2017). Consequently, the destruction of healthy tissue limits the broad capacity for using radiotherapy. In irradiated bone there is persistent cell hypoxia and delayed bone healing (Stone et al., 2003; Batista et al., 2014; Rocha et al., 2017), associated with damage to osteoprogenitor cells (Chouinard et al., 2016), reduced bone density (Mendes et al., 2019) and decreased neovascularization (Chouinard et al., 2016), favoring bone necrosis (Dieleman et al., 2017).

Hyperbaric oxygen (HBO) increases dissolved oxygen in blood plasma, reduces hypoxia and modulates the production of reactive oxygen species, which act as signaling molecules, leading to upregulation of tissue metabolism (Thom, 2009; Thom, 2011; Choudhury, 2018). HBO-mediated oxidative stress reduces inflammation (Rocha et al., 2015, stimulates the differentiation of circulating stem/progenitor cells in vitro (Lin et al., 2014; Gardin et al., 2020) and growth of new blood vessels from local endothelial cells in vivo (Grassmann et al., 2015; An et al., 2019). Furthermore, HBO has bactericidal/bacteriostatic effects (Raggio & Winters, 2018), accelerates osteoblast differentiation (Al Hadi et al., 2015), and increases expression of vascular endothelial growth factor (VEGF) (Gardin et al., 2020) and Runt-related transcription factor 2 (Runx2) (Lin et al., 2014; Rocha et al., 2015), improving bone formation (An et al., 2019; Grassmann et al., 2015; Rocha et al., 2015; Al-hadi et al., 2015; Park et al., 2019). In this context, the present study hypothesized that HBO therapy might improve repair in bone compromised by ionizing radiation. Thus, the aim of this study was to analyze the effects of HBO on bone neoformation after radiotherapy, by different methods such as assessing the histomorphometric parameters, computed tomography analysis and polarization microscopy for evaluating collagen.

2. Material and Methods

Animals and Experimental groups

This study was approved by Bioethics Committee for Animal Experimentation at the Federal University of Uberlândia (CEUA #028/12) and was conducted in accordance with the normative guidelines of the Brazilian National Council for Animal Control and Experimentation (CONCEA). Twenty healthy male Wistar rats (*Rattus norvegicus*), weighing between 250 to 350g, were used in this study. All animals were housed in standard conditions (12-hour light/dark cycle, temperature of 22±1°C and relative humidity of 50-60%), with food (composition: humidity, crude protein, ethereal extract, mineral, crude fiber,

calcium and phosphorus) and water ad libitum. After one week of acclimatization, all the animals were submitted to radiotherapy, performed on the left leg; and after 30 days, bone defects were created in both femurs. The right legs of all animals were positioned so that they remained out of the irradiation field. After this, the animals were separated into 2 groups: treated with and without HBO. Ten animals received daily sessions of HBO, and all the animals were euthanized, according to the respective group, in the time intervals of 5 or 7 days after surgery. The femurs were removed and separated into 4 groups (n=5) for each time interval of euthanasia: Control (Right femur: Non-irradiated and Non-HBO), RXT (Left femur: Irradiated and Non-HBO), HBO (Right femur: Non-irradiated with HBO), RXT+HBO (Left femur: Irradiated with HBO).

Radiotherapy, Surgical Procedure, HBO and Sample Obtainment

The animals were anaesthetized with an intraperitoneal injection of 100 mg/kg ketamine 10% and 7 mg/kg xylazine 2% hydrochloride. The left leg was positioned laterally and immobilized by means of a wooden stick and adhesive tape. A 1.5 cm thick wax bolus was placed on the left leg and dose of 30 Gy was administered in one session, using a Linear Accelerator 6MeV (Varian 600-C®, Varian Medical Systems Inc. Palo Alto California/USA). Thirty days after radiotherapy bone defects were created in both femurs as described by Batista et al. (2014).

The HBO sessions started immediately after the surgery and were applied daily for five or seven days, as described by Rocha et al. (2015). HBO therapy was carried out in a cylindrical pressure chamber (Ecobar 400, Ecotec Equipamentos e Sistemas Ltda®, Mogi das Cruzes, SP, Brazil) at 2.5 ATA for 90 minutes per session.

All animals were euthanized either 5 or 7 days after surgery, by administration of an intraperitoneal injection with sodium thiopental and lidocaine, followed by cervical dislocation, in compliance with the principles of the Universal Declaration on Animal Welfare. The diaphyses containing the bone defect were immediately fixed in PBS-buffered formalin (4%) solution (pH 7.4) for 48h at room temperature. Subsequently they were washed and stored in PBS-buffered solution, until Tomographic analysis was performed.

Computed Tomography (CT) Analysis

The samples were positioned in a standard device and scanned by means of a Cone-Beam 3D scanner (Gendex, GX-CB500-ICAT) at 7mA, 120kvp and 0,125mm voxel

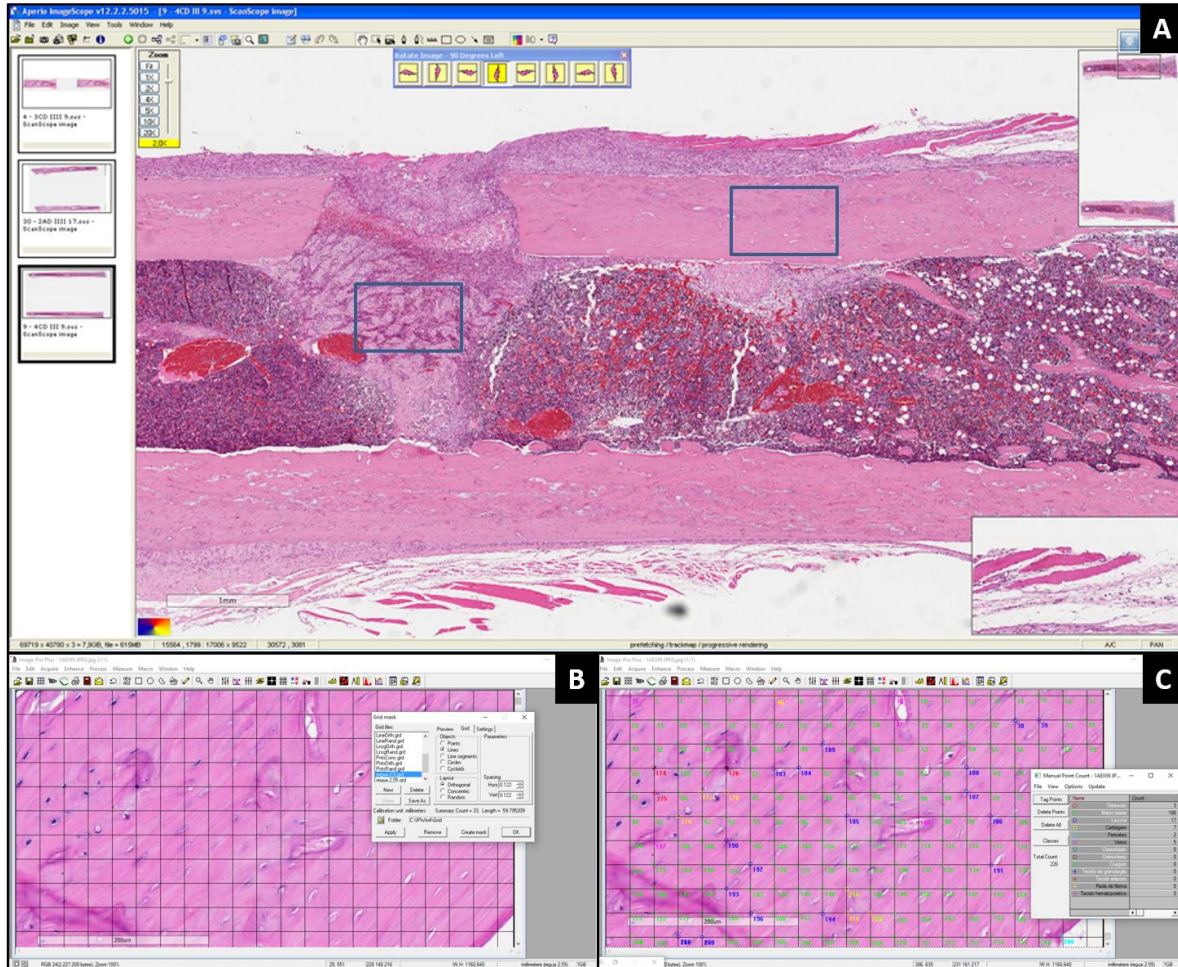
resolution. Of each femur, 3 tomographic images were selected as described by Rocha et al. (2015). The region of interest (ROI) was delimited by a rectangle, drawn from the defect edges in cortical bone to the opposite inner surface of the cortical bone. For image-specific calibration, 3 mm away from the ROI, one rectangle of 1 mm² in bone marrow region (Marrow reference) was drawn, and one in the bone cortical region (Cortical Reference). The Hounsfield scale within these three regions was assessed using specific software (i-CAT ® Vision, Imaging Sciences International, Penn Road, Hatfield, PA).

Histomorphometric Analysis

After tomographic evaluation, the bone was decalcified in 10% EDTA (pH7.2) and embedded in paraffin. The 5 µm semi-serial sections obtained were stained with Hematoxylin and Eosin (HE), Mallory Trichrome (MT) and evaluated by using optical microscopy (Optical Microscope Model Olympus® BX50, Olympus Imaging America Inc. Shinjuku-ku, Tokyo / Japan).

For histomorphometric analysis, 3 HE histological sections from each femur were scanned using the Aperio AT Turbo scanner (Copyright©Aperio Technologies, Copyright © 2013 Leica Biosystems Imaging, Inc.). In each histological image, two equal areas were delimited, one in defect region and another in cortical bone, these were 3 mm away from the defect edges. The images were analyzed by means of the Image-Pro Plus Version 4.5 program (Media Cybernetics, Silver Spring, USA). A grid with 220 points of intersection between the lines was generated and overlapped on the histological image (Figure 1).

Figure 1. Histomorphometric analysis. A- Digitized image of longitudinal section of the femur, with two areas of analysis (blue rectangle), one in defect region and another in cortical bone; B- 220-point grid generated; C- Counting of points that matches with the structures to be analyzed. HE.



Source: Authors (2020).

In Figure 1, we observe location of analyzed areas and grid delimitation for counting structures. The points that matched the components of interest in the BONE DEFECT were counted as follows: Blood Clot; Fibrin Network; Adipose Tissue; Inflammatory Cells; Granulation Tissue; Blood Vessels; Connective tissue; Bone Matrix/Osteocytes; Osteoclasts; Osteoblasts; and in CORTICAL BONE: Basophilic/amorphous Areas; Blood Vessels; Bone Matrix; Osteocytes; Empty lacunae. The results were presented in terms of density (%) according to numbered match points on the structures, within the total number of points in the grid as adapted from Vieira et al., (2015).

Also, the total bone neoformation was quantified in the defect region using 3 Mallory Trichrome stained sections for each femur, as described by Batista et al., (2014). The bone

defect (region of interest - ROI) was totally delimited with four straight lines from the edges of the injured cortical to the opposite cortical. The percentage of bone matrix within this area was quantified with the measuring tool of HL Image 2005++ (Western Vision, Salt Lake City, UT, USA).

Collagen Analysis - Polarization Microscopy

The collagen analysis was performed in 3 Picrosirius Red stained histological sections of each femur, by polarized light microscopy, using Nikon Eclipse Ti-S binocular microscope (Nikon®, Nikon Corporation, Tokyo, Japan) and the OPTHD/Opticam program coupled to a high-resolution Opticam camera (Opticam Microscopy Technology®, São José dos Campos, São Paulo, Brazil). All images were captured with a 20X objective lens against a black background, with the same light intensity and polarizing lens angle of 90° to the light source. The images were captured in the same regions of the histomorphometric analysis - bone defect and cortical.

In each image, semi-quantitative analysis was performed by two blinded examiners, using the following criteria: a) predominance of color marking, in percentage (%), whether green or yellow/orange/red. In this analysis, mature type I collagen exhibits birefringence from a yellow to reddish color, represented by the presence of thicker fibrils, while immature type III collagen is marked green; b) predominance of lamellar organization, in percentage (%), whether present or absent. In this analysis, the collagen organization was determined based on the appearance of the lamellae (Table 1). The mean values between the two examiners were considered for the analysis.

Table 1. Established criteria for evaluation.

Color Marking		Lamellar Organization	
Yellow/Orange/Red	Green	Presence	Absence
0% (Absent)	0% (Absent)	0% (Absent)	0% (Absent)
1/4 or 25% (Little)			
1/2 or 50% (Moderate)			
More than 1/2 or 50% (Abundant)			

Source: Authors (2020).

In Table 1, it is important to notice the criteria for collagen evaluation.

Statistical Analysis

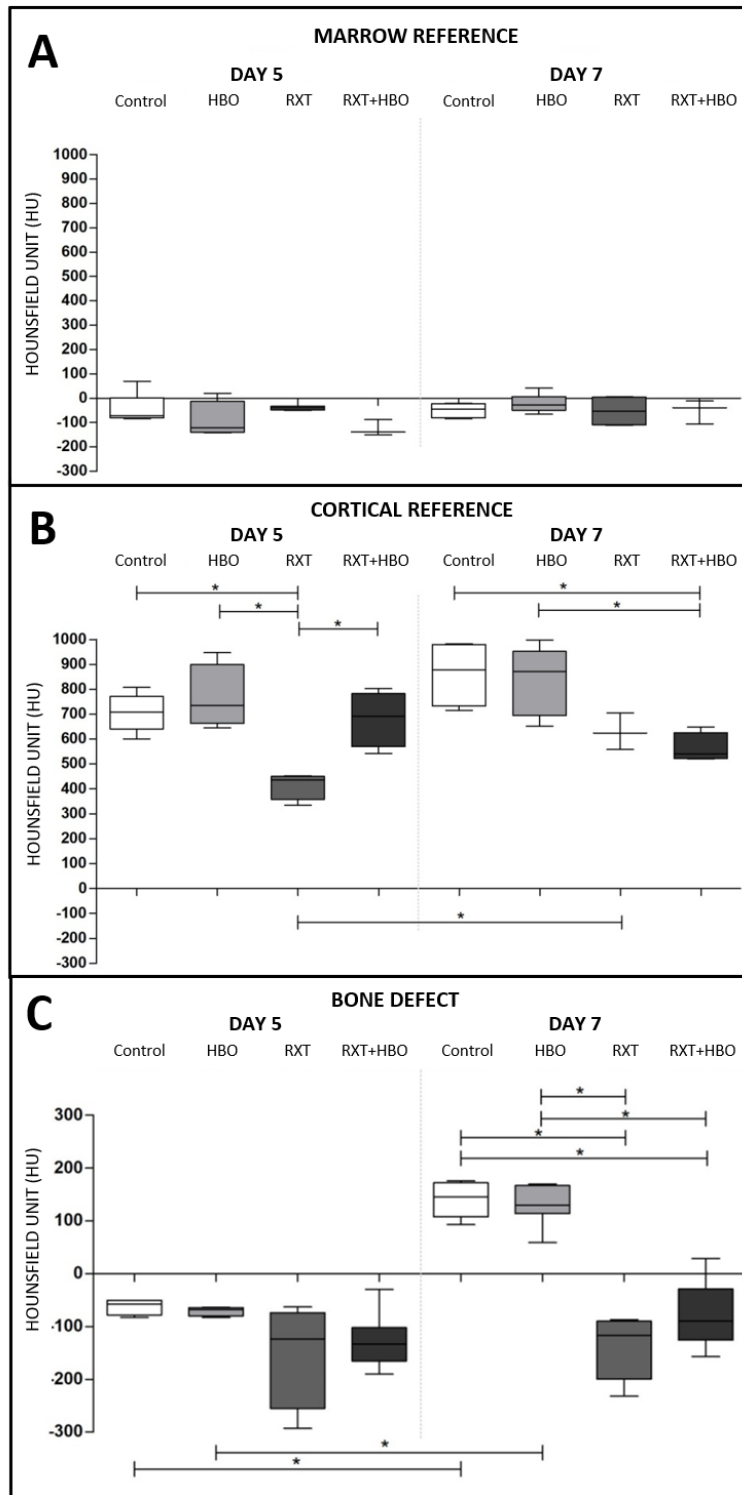
Data were analyzed using GraphPad Prism (GraphPad Prism® version 5.0 for Windows, San Diego, CA, USA). Initially, the values obtained were submitted to the Kolmogorov-Smirnov normality test. The parameters were analyzed using unpaired t-tests (for comparison of each group over time) and ANOVA with Bonferroni correction (for comparison between groups in each time interval). The differences were considered statistically significant if $p < 0.05$.

3. Results

Computed Tomographic (CT) Analysis

Bone marrow reference showed similar HU values in all groups. The cortical reference had higher HU values in Control and HBO groups in both the 5- and 7-day time intervals. Furthermore, HU values progressively increased over the time intervals in the bone defect in Control and HBO groups (Figure 2).

Figure 2. Hounsfield Unit (HU) values of evaluated groups, in 5 and 7 days. A- Bone marrow reference values; B- Cortical reference values; C- Bone defect values. (* $p < 0.05$).



Source: Authors (2020).

In Figure 2 is shown the tomographic results in cortical reference, marrow reference and bone defect, in all evaluated groups.

Histological and histomorphometry analysis

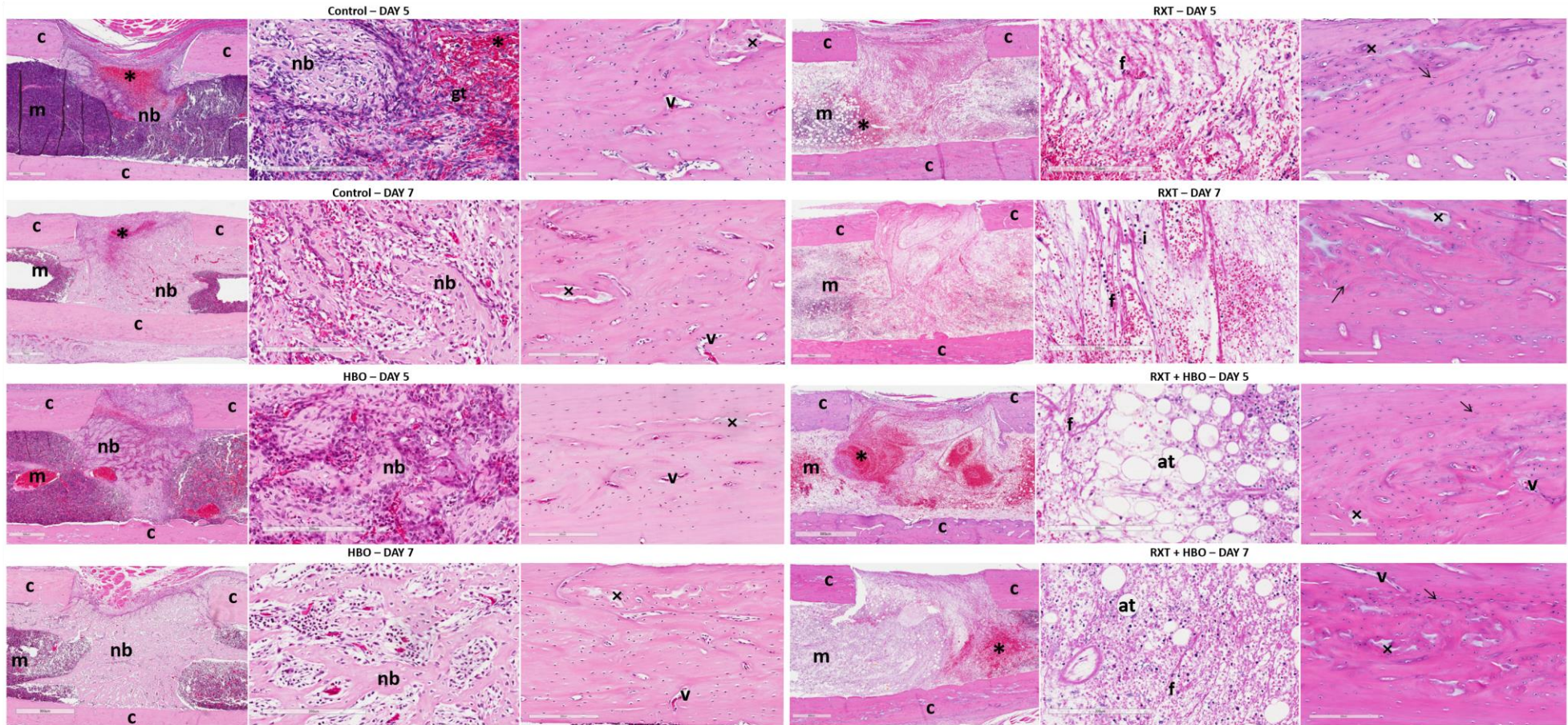
The bone defect of Control Group, at day 5, showed a reduced blood clot, and predominance of granulation tissue. Inflammatory cells and primary bone were observed in the periphery of the defect. At day 7, the defect was filled with primary bone with new vessels and few areas of granulation tissue (Figure 3).

In HBO Group, at day 5, the bone neoformation filled half of the defect area and extended into medullary canal. The primary bone had osteoblasts with cytoplasmic basophilia, and many osteocytes recently enclosed in the new bone matrix. The development of blood vessels and organized granulation tissue was observed. At day 7, the primary bone completely filled the defect area and extended largely into the medullary canal, with defined trabeculae (Figure 3).

In the groups that underwent radiotherapy several morphological alterations were observed. In bone defect area in the RXT and RXT+HBO Groups, in 5 and 7 days, no bone neoformation was observed. The defect area showed reticular fibrin network, eventual fat cells and a disorganized blood clot. Some sparse collagen fibers and chronic inflammatory infiltrate were also observed (Figure 3).

At 5 and 7 days, the cortical region in all groups showed lamellar cortical bone with channels containing blood vessels. Furthermore, in bone matrix osteocytes, empty lacunae, and basophilic lines were observed, but these were more disorganized in the RXT groups. Moreover, basophilic/amorphous areas within the bone matrix were observed in all groups, but larger number in the irradiated groups (Figure 3).

Figure 3. Histological images of bone defect and cortical region of the groups, in the 5 and 7 days. Cortical bone (c); Bone marrow (m); Newformed bone (nb); Clot (*); Granulation tissue (gt); Fibrin network (f); Inflammatory infiltrate (i); Basophilic/amorphous areas (x); Basophilic lines (black arrow); Blood vessels (v); Adipose tissue (ta). HE, X4 and X20.



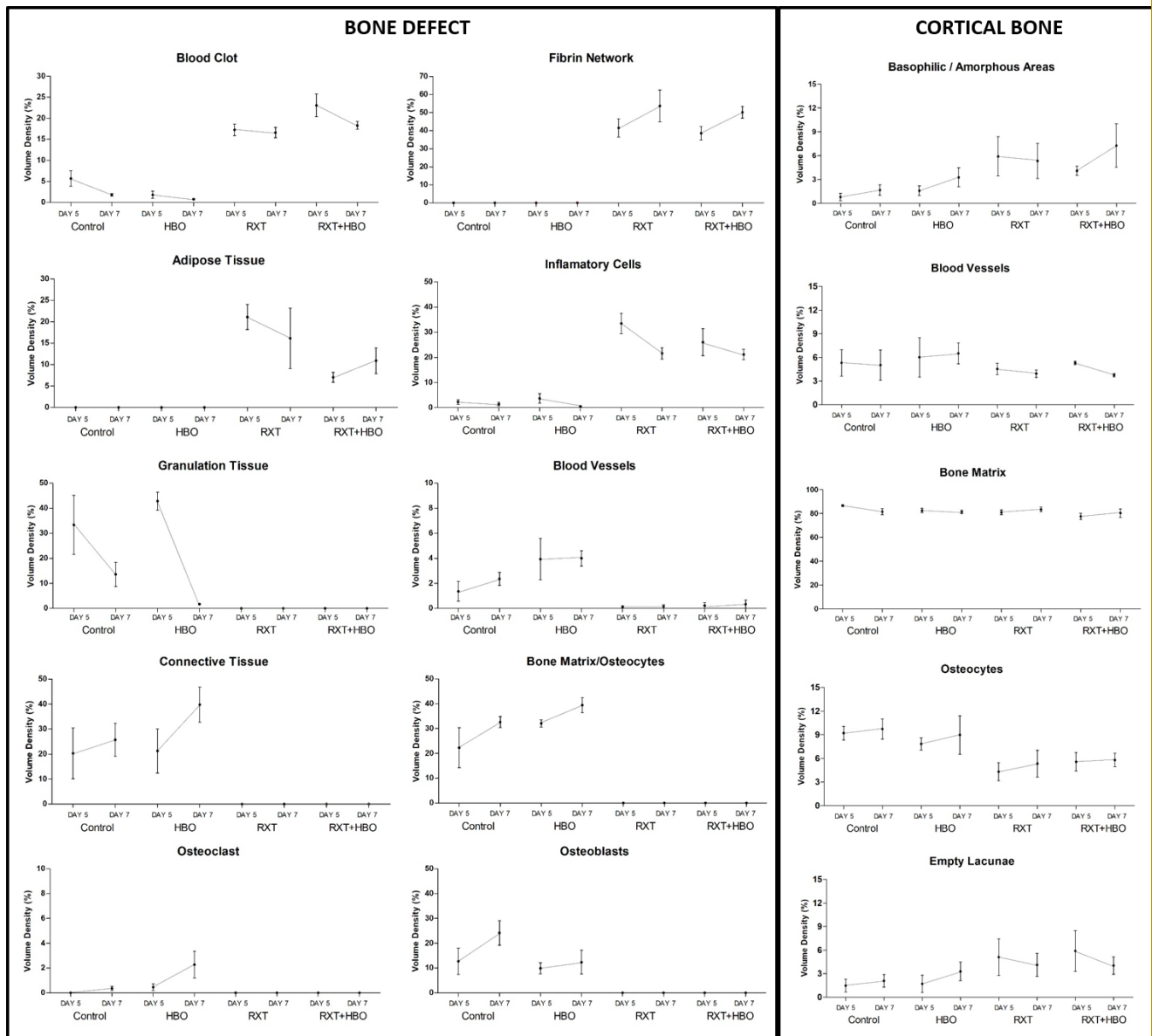
Source: Authors (2020).

Note in Figure 3 the histological images of the bone defect and cortical region of the groups, in the 5 and 7 days.

In the non-irradiated groups, histomorphometry analysis of the bone defects showed increase in bone matrix/osteocytes, osteoblasts, blood vessels, and connective tissue in both Control and HBO Groups. Osteoclasts were rarely found, but these were present in higher numbers in Group HBO in the 7 day. In the time interval between 5 and 7 days, there was a reduction in granulation tissue in both the Control and HBO groups. In the irradiated groups, (RXT and RXT+HBO) larger numbers of blood clots, fibrin networks, inflammatory cells and adipose tissues were observed (Figure 4).

In cortical region of Groups RXT and RXT+HBO, larger areas of basophilic/amorphous tissue and empty lacunae were observed. The density of the blood vessels and osteocytes was reduced in irradiated when compared with the non-irradiated groups. The bone matrix density was similar among the groups (Figure 4).

Figure 4. Histomorphometric analysis of groups, in 5 and 7 days.



In **BONE DEFECT**: Blood Clot; Fibrin Network; Adipose Tissue; Inflammatory Cells; Granulation Tissue; Blood Vessels; Connective Tissue; Bone Matrix/Osteocytes; Osteoclasts; Osteoblasts. In **CORTICAL BONE**: Basophilic/amorphous Areas; Blood Vessels; Bone Matrix; Osteocytes; Empty lacunae.

Source: Authors (2020).

Note in Figure 4 the graphs of histomorphometric analysis of the bone defect and cortical region of the groups, in the 5 and 7 days.

The statistical analysis showed significant increase in new bone formation (%) in Group HBO compared with the Control in the 5-day time interval ($p < 0.05$). There was no significant difference between Control and HBO Groups in the 7-day time interval. There was no bone formation in Groups RXT and RXT+HBO at 5 and 7 days (Table 2).

Table 2. New bone formation (%) in the ROI (bone defect) of groups, in 5 and 7 days.

Time Intervals	Groups	New bone formation (%)
DAY 5	Control	7.06 ± 3.71*
	HBO	15.95 ± 7.68*
	RXT	0
	RXT+HBO	0
DAY 7	Control	23.10 ± 7.40
	HBO	28.10 ± 5.40
	RXT	0
	RXT+HBO	0

Source: Authors (2020).

In Table 2, it is important to notice that in irradiated groups, no bone formation was observed.

Collagen Analysis

In Group HBO, predominance of Yellow/Orange/Red collagen material was observed both in the defect and cortical areas, in the 5- and 7-day time intervals ($p < 0.05$). In Groups Control, RXT and RXT+HBO, predominant Green birefringence was observed in the bone defect region, indicating the presence of type III collagen in the 5- and 7-day time intervals. Only Group HBO showed predominant Yellow/Orange/Red birefringence in the bone defect in the 5- and 7-day time intervals ($p < 0.05$) (Figure 5).

In all groups, lamellar organization of collagen bundles was observed mainly near the bone surface and less frequently within cortical bone. Whereas in the bone defect, collagen bundles with lamellar organization were rarely observed, with Groups Control and HBO showing significant difference when compared with Groups RXT and RXT+HBO ($p < 0.05$) (Figure 5).

Note in Figure 5 the differences in collagen of the bone defect and cortical region of the groups, in the 5 and 7 days.

4. Discussion

This study investigated the effect of HBO on bone repair and collagen orientation after radiation exposure in an animal model. Deleterious effects of ionizing radiation on bone tissue can persist for long periods and the complications in irradiated bone appear to be dose dependent (Lerouxel et al., 2009; Limírio et al., 2019). The single dose of 30 Gy radiation has previously been used in other studies of our group (Batista et al. 2014, Rocha et al., 2017; Soares et al., 2018; Limirio et al., 2019). This higher dose increases the risk of ORN (Dieleman et al., 2017) when compared with doses of 50-70 Gy, indicated for cancer treatment by multifractionated delivery (Ohrnell et al., 1997; Lerouxel et al., 2009). Thus, the single dose of 30 Gy was sufficient to cause bone damage, allowing the repair of bone in poor conditions to be evaluated (Batista et al. 2014, Rocha et al., 2017; Soares et al., 2018; Limirio et al., 2019). Although higher radiation doses would increase the probability of ORN occurring (Lerouxel et al., 2009), surprisingly, in our study no animals developed osteonecrosis. Apparently, the development of ORN may require more time for significant cumulative radiation damage to appear (Dieleman et al., 2017). In addition, the environment of the femur differs from that of the oral cavity, as it has a smaller bacterial population, which may have contributed to our results.

The primary effect of radiation on bone is atrophy, with a marked reduction in its functional components and decline in repair capacity (Hopewell, 2003; Lerouxel et al., 2009). The body itself is incapable of repairing the damage, and the severe blood vessel atrophy results in loss of bone cells, dysregulated interactions between cell populations and hypoxia (Stone et al., 2003). Supposing that bone requires increased cell proliferation to achieve healing, our results confirmed existing findings that radiation significantly reduced the bone healing process (Stone et al., 2003; Batista et al., 2014; Rocha et al., 2017). Specifically, irradiated bone marrow-derived mesenchymal stem cells (BMSCs) have exhibited declined viability and impaired osteogenic differentiation (Bai et al., 2020; Chouinard et al., 2016), with reduced bone cell phenotype replacement (Bai et al., 2020), as observed in Group RXT. The reduction in BMSCs post-irradiation could be one of the important causes of radiation-induced bone deterioration (Bai et al., 2020).

In this sense, HBO treatment in irradiated tissues is interesting, because it enhances

the growth of new blood vessels (Grassmann et al., 2015; An et al., 2019) and osteogenic differentiation of mesenchymal stem cells (Lin et al., 2014; Gardin et al., 2020) thereby accelerating repair (Rocha et al., 2015). However, in our study, bone healing was markedly compromised after radiotherapy, and HBO failed to reverse the damage. In fact, in Group RXT+HBO, we also observed a reduction in blood vessels and bone cells; no bone formation was found, and the defect was filled with loose, poorly organized tissue. These results are conflicting with others who have demonstrated improved bone regeneration (Park et al., 2019) and angiogenesis (An et al., 2019) in irradiated (12Gy single dose) calvaria defects after HBO treatment. This most probably occurred due to different experimental models, considering that damage by radiation occurs in a dose-dependent manner (Lerouxel et al., 2009; Limirio et al., 2019; Bai et al., 2020). To our knowledge, the main target for the physiological action of HBO is tissue hypoxia (Choudhury et al., 2018). However, it is possible that after high doses of radiation, such as applied in our study, angiogenic impairment was so great that vascular response remained low and the oxygen perfusion in the bone defect was insufficient to correct the cellular imbalance (Jerezek-Fossa et al., 2002; Choudhury et al., 2018). Unfortunately, this is one of the limitations of HBO treatment, as oxygen can only be locally delivered to areas receiving adequate blood supply (Choudhury et al., 2018). Perhaps, significant vascular recovery after high dose radiotherapy requires a higher number of HBO sessions.

In the present study, the contralateral non-irradiated femurs were used as Control and HBO groups, in a paired study, for comparison with Groups RXT and RXT+HBO, considering that alterations in bone repair caused by radiation are not observed at sites far from the irradiated field (Rocha et al., 2017). In Control Group, repair occurred as intended and HBO clearly accelerated the initial events of bone healing. In Group HBO, there was increase in blood vessels, bone neoformation and collagen maturation when compared with the other groups. New blood vessel formation is an important condition for adequate bone repair, since it allows local oxygenation, delivers nutrients, removes waste products, and provides cells and mediators (Sirin, 2011). During HBO, the amount of oxygen dissolved in the plasma occurs resulting in hyperoxygenation of tissues. This leads to intracellular generation of reactive oxygen species (ROS) and nitrogen, activating oxygen mediated oxidative stress (Thom, 2009; Thom, 2011; Choudhury et al., 2018). Soon after the end of the session, PO₂ returns to normal levels and the chemical mediators released stimulate cellular functions with enhanced angiogenesis, rapid resolution of inflammation, collagen synthesis and osteogenesis (Thom, 2009; Thom, 2011; Rocha et al., 2015; Choudhury et al., 2018), similar to our findings. This is in agreement with the studies of Wang et al. (2005) and

Kawada et al. (2013) in which HBO improved osteoblast function when applied during the early stages of bone healing, with increased expression of VEGF (Gardin et al., 2020, type I collagen (Al Hadi et al., 2015 and Runx-2 (Rocha et al., 2015, Al Hadi et al., 2015). It seems feasible to think that in Group HBO, nutrients were delivered more rapidly to the tissue by newly formed vessels, allowing better bone repair and cell function.

Bone undergoing healing usually contains a substantial amount of immature collagen, which is later replaced by mature collagen (Vieira et a., 2015; Mendes et al., 2019). Given this fact, a smaller amount of mature collagen would indicate more immaturity of newformed bone. There is strong evidence that collagen synthesis and maturation is dependent on oxygen supply (Sen, 2009; Gajendrareddy et al 2017), as hyperoxia stimulates the synthesis of basic fibroblast growth factor (bFGF) (Thom, 2009; Thom, 2011), favoring bone matrix production. This may have contributed to our results demonstrating predominance of mature type I collagen (yellow to reddish color) after HBO in the cortical bone and defect. Other authors have demonstrated that HBO improved collagen maturation in bone (Limirio et al., 2018) and in the periodontal ligament (Gajendrareddy et al., 2017). Nevertheless, our collagen results should be interpreted with caution because polarized light measurements were applied to assess the collagen color, predominance, and arrangement, but not in a fully quantitative way.

It is well accepted that bone exhibits birefringence dependent upon the composition and orientation of its collagen, with differences in brightness observed by polarized light microscopy (Bromage 2003). However, it must be considered that mineralized collagen bundles in natural bone are made up of collagen fibrils and hydroxyapatite mineral crystals, which function as a unit in the bone structure (Georgiadis et al., 2016). The images obtained by the polarization method are susceptible to changes depending on the collagen content/density (i.e. matrix-to-mineral ratio) (Bromage 2003, Georgiadis et al., 2016), which are not uniform throughout a bone section. As such, our findings obtained from demineralized slides allowed limited comparative evaluation of collagen in bone, as hydroxyapatite mineral crystals were removed, which could lead to incorrect interpretations when used without other parameters. In fact, it is suggested that radiation induced specific changes in the collagen mature/immature crosslink ratio, and collagen/hydroxyapatite ratio (Limirio et al., 2019). But it has not yet been elucidated whether these changes might also be found after HBO treatment.

An interesting finding in the cortical region, was the larger number of basophilic/amorphous areas and evident lamellar disorganization in the irradiated groups. These findings agreed with those of Rabelo et al. (2010), who found reduction in bone matrix

and high heterogeneity in the microarchitecture of Harvers channels after radiotherapy, revealing less organized bone. Although the cartilaginous nature of these areas was not confirmed in the present study, we hypothesized that these basophilic/amorphous areas would be similar to highly calcified cartilage islands found by Shipov et al. (2013) and Bach-Gansmo et al. (2013) within rat cortical bone. The authors suggested that these disorganized regions represented residual areas of endochondral ossification that were not remodeled, not resorbed, and not replaced by lamellar bone on rat maturity (Shipov et al., 2013; Bach-Gansmo et al., 2013). The increased occurrence of such areas, accompanied by lamellar disorganization in irradiated groups, indicated compromised endochondral ossification due to radiation, as previously reported by Rocha et al. (2016).

The cone beam tomography, used in this study, is often associated with degradation of grayscale fidelity of the image finally displayed (Molteni et al., 2013; Pawels et al., 2015). In general, smaller irradiated volumes, such as those used in our study, are less prone to inaccurate CT numbers/HU, caused by scattered radiation and by non-ideal geometry (Molteni et al., 2013). But even with appropriate image acquisition, care should be taken when interpreting quantitative measurements of density obtained with cone beam tomography. Despite these limitations, the method provided important information. Our CT findings demonstrated greater HU values only at 7 days in Control and HBO groups suggesting mineralization of the new formed bone in this time interval. Usually, repair must enter the late stage of osteogenesis to present mineralized bone resulting in higher HU values. The chronology of bone healing is characterized by the presence of clot; migration and proliferation of MSCs; granulation tissue formation with infiltration of inflammatory cells, angiogenesis, proliferation of fibroblasts and collagen synthesis; and, finally, bone formation and remodeling (Vieira et al., 2015).

In the present study, after radiotherapy, the greatest differences occurred in the defect rather than cortical bone, as expected. The first events are usually cellular and vascular (Hopewell, 2003; Lerouxel et al., 2009), followed by damage to the remodeling system and then, to bone structure (Rabelo et al., 2010; Soares et al., 2018; Limirio et al., 2019). It would appear that the effects of radiation on bone tissue structure (cortical bone) should take place in some period after the radiation exposure, rather than immediately (Soares et al., 2018; Limirio et al., 2019). This is related to the time elapsed between the time when the cellular and vascular changes occur (immediately) and the time when significant impairment can be seen in macroscopic bone morphology and architecture.

4. Conclusion

Our results indicated that HBO improved bone repair and collagen arrangement in physiological conditions, with increased blood vessels and bone neoformation. However, HBO did not improve the repair of bone after the high ionizing radiation dose. It is necessary to establish more standardized protocols for this therapy, with longer periods of evaluation. Thus, future studies should be performed in order to clarify the role of HBO in bone after radiotherapy.

Acknowledgments

The authors would like to thank FAPEMIG for the research grants FAPEMIG APQ-00998-14; School of Medicine of the Federal University of Triângulo Mineiro (UFTM) for support in ionizing radiation procedures; Bioterismo and Animal Experimentation Center – UFU for support in animal care.

References

- Al Hadi, H., Smerdon, G. R., Fox, S. W. (2015) Hyperbaric oxygen therapy accelerates osteoblast differentiation and promotes bone formation. *J Dent.* 3(3), 382-8. doi: 10.1016/j.jdent.2014.10.006.
- An, H., Lee, J. T., Oh, S. E., Park, K. M., Hu, K. S., Kim, S., Chung, M. K. (2019) Adjunctive hyperbaric oxygen therapy for irradiated rat calvarial defects. *J Periodontal Implant Sci.* 49(1), 2–13. doi: 10.5051/jpis.2019.49.1.2
- Bach-Gansmo, F. L., Irvine, S. C., Brüel, A., Thomsen, J. S., Birkedal, H. (2013) Calcified cartilage islands in rat cortical bone. *Calcif Tissue Int.* 92(4), 330-8. doi: 10.1007/s00223-012-9682-6.
- Bai, J., Wang, Y., Wang, J., Zhai, J., He, F., Zhu, G. (2020) Irradiation-induced senescence of bone marrow mesenchymal stem cells aggravates osteogenic differentiation dysfunction via paracrine signaling. *Am J Physiol Cell Physiol.* 318(5), C1005-C1017. doi: 10.1152/ajpcell.00520.2019.

Batista, J. D., Zanetta-Barbosa, D., Cardoso, S. V., Dechichi, P., Rocha, F. S., Pagnoncelli, R. M. (2014) Effect of low-level laser therapy on repair of the bone compromised by radiotherapy. *Lasers Med Sci.* 29(6), 1913-8. doi: 10.1007/s10103-014-1602-8.

Bromage, T. G., Goldman, H. M., McFarlin, S. C., Warshaw, J., Boyde, A., Riggs, C. M. (2003) Circularly polarized light standards for investigations of collagen fiber orientation in bone. *Anat Rec B New Anat.* 274(1), 157-68. doi: 10.1002/ar.b.10031.

Choudhury, R. (2018) Hypoxia and hyperbaric oxygen therapy: A review. *International Int J Gen Med.* 11, 431–442. doi: 10.2147/IJGM.S172460.

Chouinard, A. F., Giasson, L., Fortin, M. (2016) Hyperbaric Oxygen Therapy for Head and Neck Irradiated Patients with Special Attention to Oral and Maxillofacial Treatments. *J Can Dent Assoc.* 82, g24. Retrieved from <https://jcda.ca/g24>.

Dieleman, F. J., Phan, T. T. T., van den Hoogen, F. J. A., Kaanders, J. H. A. M., Merckx, M. A. W. (2017) The efficacy of hyperbaric oxygen therapy related to the clinical stage of osteoradionecrosis of the mandible. *Int J Oral Maxillofac Surg.* 46(4), 428-433. doi: 10.1016/j.ijom.2016.12.004.

Gajendrareddy, P. K., Junges, R., Cygan, G., Zhao, Y., Marucha, P. T., Engeland, C. G. (2017) Increased oxygen exposure alters collagen expression and tissue architecture during ligature-induced periodontitis. *J Periodontal Res.* 52(3), 644–649. doi: 10.1111/jre.12408.

Gardin, C., Bosco, G., Ferroni, L., Quartesan, S., Rizzato, A., Tatullo, M., Zavan, B. (2020) Hyperbaric Oxygen Therapy Improves the Osteogenic and Vasculogenic Properties of Mesenchymal Stem Cells in the Presence of Inflammation In Vitro. *Int J Mol Sci.* 20;21(4), 1452. doi: 10.3390/ijms21041452.

Georgiadis, M., Müller, R., Schneider, P. (2016) Techniques to assess bone ultrastructure organization: orientation and arrangement of mineralized collagen fibrils. *J R Soc Interface.* 13(119), 20160088. doi: 10.1098/rsif.2016.0088.

Grassmann, J. P., Schnependahl, J., Hakimi, A. R., Herten, M., Betsch, M., Lögters, T. T., Thelen, S., Sager, M., Wild, M., Windolf, J., Jungbluth, P., Hakimi, M. (2015) Hyperbaric oxygen therapy improves angiogenesis and bone formation in critical sized diaphyseal defects. *J Orthop Res.* 33(4), 513-20. doi: 10.1002/jor.22805.

Hopewell, J. W. (2003) Radiation-therapy effects on bone density. *Med Pediatr Oncol.* 41(3), 208-11. doi: 10.1002/mpo.10338.

Jereczek-Fossa, B. A., Orecchia, R. (2002) Radiotherapy-induced mandibular bone complications. *Cancer Treat Rev.* 28(1), 65-74. doi: 10.1053/ctrv.2002.0254.

Kawada, S., Wada, E., Matsuda, R., Ishii, N. (2013) Hyperbaric Hyperoxia Accelerates Fracture Healing in Mice. *Plos ONE* 8(8), e72603.

Lerouxel, E., Moreau, A., Bouler, J. M., Giumelli, B., Daculsi, G., Weiss, P., Malard, O. (2009) Effects of high doses of ionising radiation on bone in rats: a new model for evaluation of bone engineering. *Br J Oral Maxillofac Surg.* 47(8), 602-607. doi: 10.1371/journal.pone.0072603

Limirio, P. H. J. O., da Rocha Junior, H. A., Morais, R. B., Hiraki, K. R. N., Balbi, A. P. C., Soares, P. B. F., Dechichi, P. (2018) Influence of hyperbaric oxygen on biomechanics and structural bone matrix in type 1 diabetes mellitus rats. *PLoS One.* 13(2), e0191694. doi: 10.1371/journal.pone.0191694

Limirio, P. H. J. O., Soares, P. B. F., Emi, E. T. P., Lopes, C. C. A., Rocha, F. S., Batista, J. D., Rabelo, G. D., Dechichi, P. (2019) Ionizing radiation and bone quality: time-dependent effects. *Radiat Oncol.* 14(1), 15. doi: 10.1186/s13014-019-1219-y.

Lin, S. S., Ueng, S. W., Niu, C. C., Yuan, L. J., Yang, C. Y., Chen, W. J., Lee, M. S., Chen, J. K. (2014) Effects of hyperbaric oxygen on the osteogenic differentiation of mesenchymal stem cells. *BMC Musculoskelet Disord.* 25;15, 56. doi: 10.1186/1471-2474-15-56.

Mendes, E. M., Irie, M. S., Rabelo, G. D., Borges, J. S., Dechichi, P., Diniz, R. S., Soares, P. B. F. (2019) Effects of ionizing radiation on woven bone: influence on the osteocyte lacunar

network, collagen maturation, and microarchitecture. *Clin Oral Investig.* 24, 2763–2771. doi: 10.1007/s00784-019-03138-x.

Molteni, R. (2013) Prospects and challenges of rendering tissue density in Hounsfield units for cone beam computed tomography. *Oral Surg Oral Med Oral Pathol Oral Radiol.* 116(1), 105-19. doi: 10.1016/j.oooo.2013.04.013.

Ohrnell, L. O., Branemark, R., Nyman, J., Nilsson, P., Thomsen, P. (1997) Effects of irradiation on the biomechanics of osseointegration. An experimental in vivo study in rats. *Scandinavian journal of plastic and reconstructive surgery and hand surgery.* 31(4), 281-93. doi: 10.3109/02844319709008974.

Park, K. M., Kim, C., Park, W., Park, Y. B., Chung, M. K., Kim, S. (2019) Bone Regeneration Effect of Hyperbaric Oxygen Therapy Duration on Calvarial Defects in Irradiated Rats. *Biomed Res Int.* 2019; 9051713. doi: 10.1155/2019/9051713.

Pauwels, R, Jacobs, R., Singer, S. R. Mupparapu M. (2015) CBCT-based bone quality assessment: are Hounsfield units applicable? *Dentomaxillofac Radiol.* 44(1):20140238. doi: 10.1259/dmfr.20140238.

Rabelo, G. D., Beletti, M. E., Dechichi, P. (2010) Histological analysis of the alterations on cortical bone channels network after radiotherapy: A rabbit study. *Microsc Res Tech.* 73(11), 1015-8. doi: 10.1002/jemt.20826.

Raggio, B. S., Winters, R. (2018) Modern management of osteoradionecrosis. *Curr Opin Otolaryngol Head Neck Surg.* 26(4), 254-259. doi: 10.1097/MOO.0000000000000459.

Rocha, F. S., Dias, P. C., Limirio, P. H., Lara, V. C., Batista, J. D., Dechichi, P. (2017) High doses of ionizing radiation on bone repair: is there effect outside the irradiated site? *Injury.* 48(3), 671-673. doi: 10.1016/j.injury.2016.11.033.

Rocha, F. S., Gomes Moura, C. C., Rocha Rodrigues, D. B., Zanetta-Barbosa, D., Nakamura Hiraki, K. R., Dechichi, P. (2015) Influence of hyperbaric oxygen on the initial stages of bone

healing. *Oral Surg Oral Med Oral Pathol Oral Radiol.* 120(5), 581-587. doi: 10.1016/j.oooo.2015.06.039.

Rocha, F. S., Limirio, P. H., Zanetta-Barbosa, D., Batista, J. D., Dechichi, P. (2016) The effects of ionizing radiation on the growth plate in rat tibiae. *Microsc Res Tech.* 79(12), 1147-1151. doi: 10.1002/jemt.22769.

Sen, C. K. (2009) Wound healing essentials: let there be oxygen. *Wound Repair Regen.* 17(1), 1–18. doi: 10.1111/j.1524-475X.2008.00436.x.

Shipov, A., Zaslansky, P., Riesemeier, H., Segev, G., Atkins, A., Shahar, R. (2013) Unremodeled endochondral bone is a major architectural component of the cortical bone of the rat (*Rattus norvegicus*). *J Struct Biol.* 183(2), 132-40. doi: 10.1016/j.jsb.2013.04.010

Sirin, Y., Olgac, V., Dogru-Abbasoglu, S., Tapul, L., Aktas, S., Soley, S. (2011) The influence of hyperbaric oxygen treatment on the healing of experimental defects filled with different bone graft substitutes. *Int J Med Sci.* 8(2), 114–125. doi: 10.7150/ijms.8.114.

Soares, P. B. F., Soares, C. J., Limirio, P. H. J. O., de Jesus, R. N. R., Dechichi, P., Spin-Neto, R., Zanetta-Barbosa, D. (2019) Effect of ionizing radiation after-therapy interval on bone: histomorphometric and biomechanical characteristics. *Clin Oral Investig.* 23(6), 2785-2793. doi: 10.1007/s00784-018-2724-3.

Sroussi, H. Y., Epstein, J. B., Bensadoun, R. J., Saunders, D. P., Lalla, R. V., Migliorati, C. A., Heavilin, N., Zumsteg, Z. A. (2017) Common oral complications of head and neck cancer radiation therapy: mucositis, infections, saliva change, fibrosis, sensory dysfunctions, dental caries, periodontal disease, and osteoradionecrosis. *Cancer Med.* 6(12), 2918-2931. doi: 10.1002/cam4.1221.

Stone, H. B., Coleman, C. N., Anscher, M. S., McBride, W. H. (2003) Effects of radiation on normal tissue: consequences and mechanisms. *Lancet Oncol.* 4(9), 529-36. doi: 10.1016/s1470-2045(03)01191-4.

Thom, S. R. (2011) Hyperbaric oxygen: its mechanisms and efficacy. *Plast Reconstr Surg* 127(Suppl 1), 131S–141S. doi: 10.1097/PRS.0b013e3181f8e2bf.

Thom, S. R. (2009) Oxidative stress is fundamental to hyperbaric oxygen therapy. *J Appl Physiol*. 106(3), 988-95. doi: 10.1152/jappphysiol.91004.2008.

Vieira, A. E., Repeke, C. E., Ferreira Junior, S. B., Colavite, P. M., Biguetti, C. C., Oliveira, R. C., Assis, G. F., Taga, R., Trombone, A. P., Garlet, G. P. (2015) Intramembranous bone healing process subsequent to tooth extraction in mice: micro-computed tomography, histomorphometric and molecular characterization. *PLoS One*. 10(5), e0128021. doi: 10.1371/journal.pone.0128021.

Wang, I. C., Wen-Neng Ueng, S., Yuan, L. J., Tu, Y. K., Lin, S. S., Wang, C. R., Tai, C. L., Wang, K. C. (2005) Early administration of hyperbaric oxygen therapy in distraction osteogenesis: a quantitative study in New Zealand rabbits. *The Journal of Trauma*. 58(6), 1230-5. doi: 10.1097/01.ta.0000169872.38849.b0.

Percentage of contribution of each author in the manuscript

Flaviana Soares Rocha – 25%

Layra Gabriella Pereira de Rezende – 15%

Danyella Carolyna Soares dos Reis – 15%

Gustavo Davi Rabelo – 5%

Letícia de Souza Castro Filice – 5%

Darceny Zanetta-Barbosa – 10%

Paula Dechichi – 25%